DR2005161

GSA Data Repository material: Sinha et al., Variability of Southwest Indian Summer Monsoon precipitation during the Bølling-Ållerød

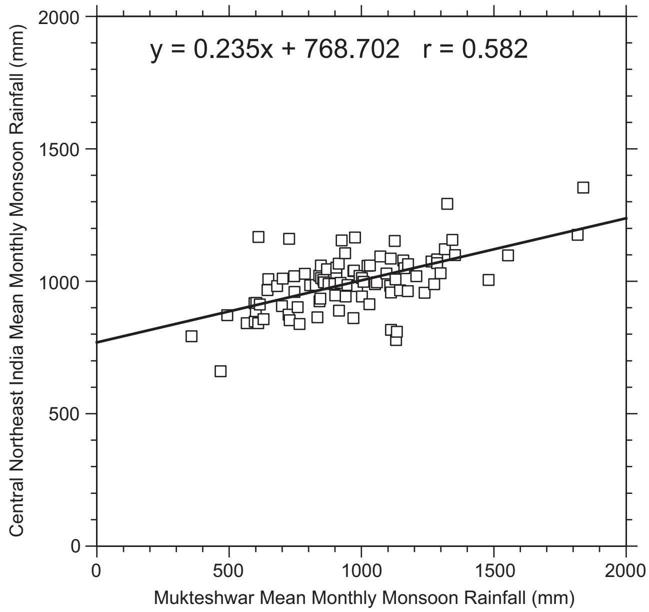

Figure DR1. Correlation of mean monthly monsoon rainfall (1901 A.D. to 1990 A.D.) near Timta Cave (Mukteshwar meteorological station, 29.28˚N; 79.39˚W, elevation 2000 m) to area weighted monsoon rainfall in Central Northeast India (Indian Meteorology Department). Monsoon rainfall in Central Northeast India indicative of overall strength of Bay of Bengal monsoon branch. During stronger (weaker) monsoons, the intensified (weakened) depressions from the Bay of Bengal bring greater (lesser) fraction of moisture to this region resulting in higher (lower) than average precipitation.

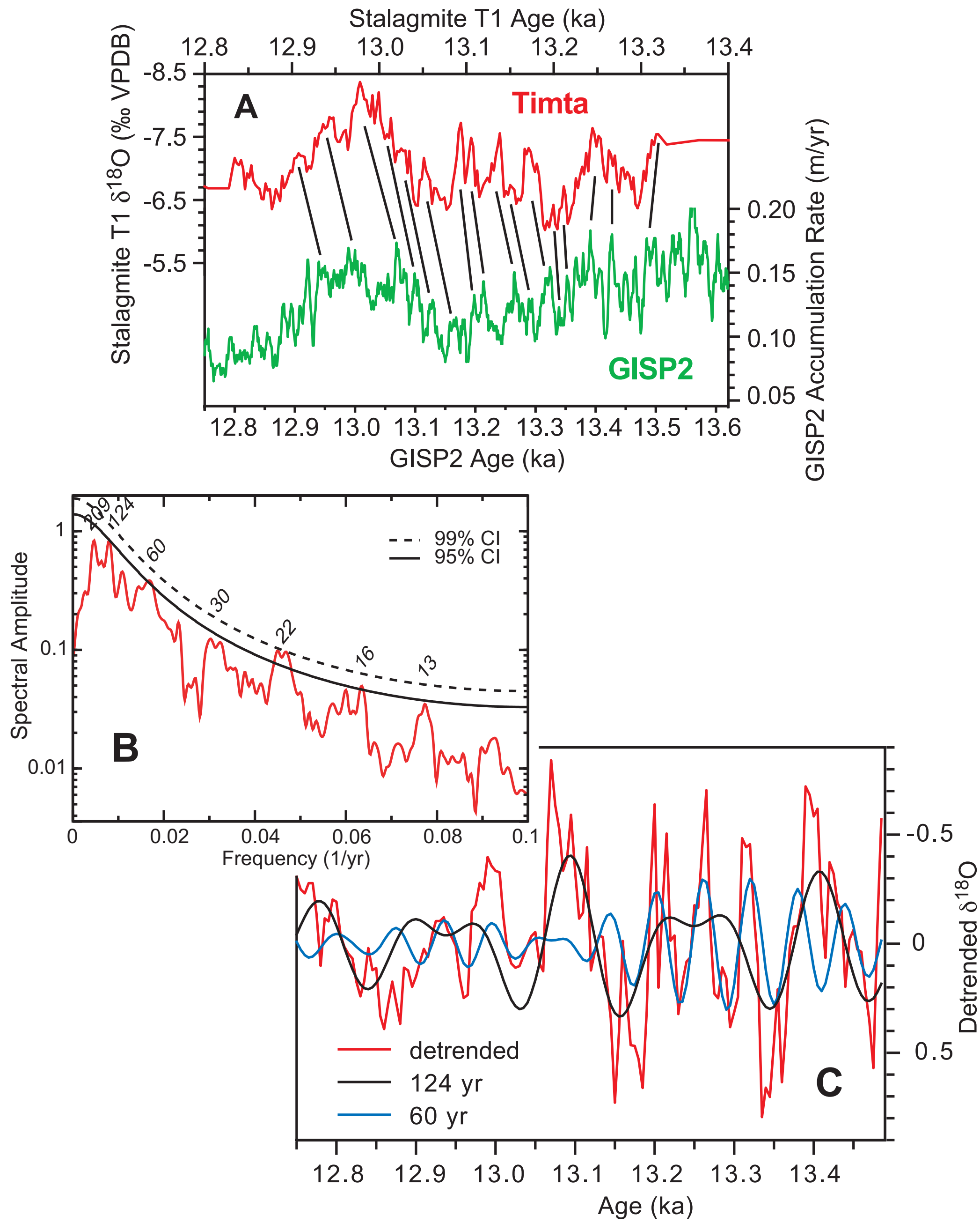

Figure DR2. (A) Tuning of stalagmite T1 δ^{18}O record to GISP2 accumulation rate record (Alley et al., 1993). Black lines indicate correlative events. (B) Power spectrum of stalagmite T1 δ^{18}O record (Ghil et al., 2002) computed using the multi-taper method (time bandwidth product of 3, 5 tapers, and robust red noise estimation to the logarithm of the spectrum). Record was detrended prior to analysis by removing 1st reconstructed component determined by singular spectrum analysis. Chisquared confidence intervals of 99% (dashed) and 95% (solid) of the power spectrum estimates. Spectral peaks significant above the 95% level are labeled with their period (yr). (C) Comparison of detrended stalagmite T1 d18O record with the reconstructed components (Ghil et al., 2002) of 124 and 60 yr periods.

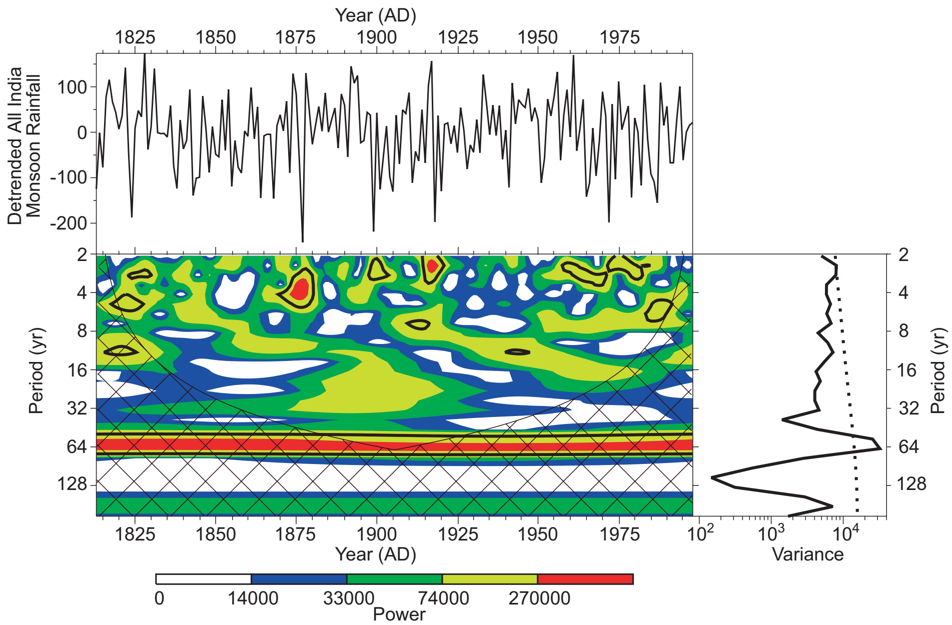

Figure DR3: All India monsoon rainfall (top) (Sontakke et al., 1993) wavelet power spectrum (bottom left) (Torrence and Compo, 1998). The contour levels are chosen so that 75%, 50%, 25%, and 5% of the wavelet power is above each level, respectively. The cross-hatched region is the cone of influence, where zero padding has reduced the variance. Black contour is the 90% confidence interval, using a red-noise (autoregressive lag1) background spectrum. The global wavelet power spectrum is shown on the right (black line). The dashed line is the 90% confidence interval.

Table DR1. ^{230}Th dating of stalagmite T1 from Timta Cave by magnetic sector inductively coupled plasma mass spectrometry. Errors are 2σ. Decay constant values are λ_{230} = 9.1577 x 10^{-6} y^{-1}, λ_{234} = 2.8263 x 10^{-6} y^{-1}, λ_{238} = 1.55125 x 10^{-10} y^{-1}. Corrected ^{230}Th ages assume the initial ^{230}Th/^{232}Th atomic ratio of 3.0 ±1.5 x 10^{-6}. This correction is different from the standard value of 4.4 ppm. This value was determined by the measurements of 2 or 3-point isochrons (T1-6, T1-7 and T1-8) and it was constrained well by those samples from the same layer (same age) with different measured ^{230}Th/^{232}Th values. The arbitrarily assumed error (50%) covers all possible ranges of the initial ^{230}Th/^{232}Th values constrained by the three isochrons. The chemical separation procedures at the University of Minnesota Isotope Laboratory are similar to those described by Edwards et al. (1987). The bias corrections and half-lives of ^{230}Th and ^{234}U followed Cheng et al. (2000). Thorium and uranium isotopes were analyzed separately on a Finnigan-MAT Element outfitted with a double focusing sector-field magnet in reversed Nier-Johnson geometry and a single MasCom multiplier. The instrument was operated in low resolution and in electrostatic peak hopping mode. Combined ionization plus transmission efficiency of 2.5 to 3‰ has been measured for uranium and 1.5 to 2‰ has been measured for thorium. Further details of instrumental procedures are explained by Shen et al. (2002). Depths are relative to the top (youngest surface) of the stalagmite. Ages are relative to 1950 AD.

Sample Number	Distance (cm)	^{238}U (ppb)	^{232}Th (ppt)	^{230}Th/^{232}Th (atomic x 10^{-6})	δ^{234}U* (measured)	^{230}Th/^{238}U (activity)	^{230}Th Age (yr) (uncorrected)	^{230}Th Age (yr) (corrected)	$\delta^{234}U_{Initial}$** (corrected)
T1-1a	0.113	176.1 ±0.3	2135 ±20	158 ±3	109.2. ±2.6	0.1159 ±0.0016	12030 ±170	**11820 ±210**	112.9 ±2.7
T1-1b	0.113	222.2 ±0.5	5060 ±30	84 ±1	108.4 ±2.7	0.1161 ±0.0017	12070 ±170	**11660 ±270**	112.0 ±2.8
T1-178-180	0.113	216.7 ±0.5	13200 ±38	33.3 ±0.3	110.5 ±2.1	0.1230 ±0.0011	12800 ±125	**11710 ±560**	114.2 ±2.1
T1-2a	1.800	243.6 ±0.5	5580 ±34	91 ±1	107.7 ±3.0	0.1256 ±0.0018	13120 ±200	**12710 ±290**	111.6 ±3.2
T1-2b	1.800	255.1 ±0.5	5010 ±32	105 ±1	105.4 ±2.9	0.1251 ±0.0015	13090 ±170	**12740 ±250**	109.3 ±3.0
T1-221-223	1.813	187.2 ±0.3	3210 ±13	124 ±1	109.1 ±1.8	0.1290 ±0.0010	13475 ±120	**13140 ±210**	113.2 ±1.9
T1-3	2.200	134.0 ±0.3	1425 ±22	194 ±4	100.3 ±3.4	0.1251 ±0.0020	13160 ±220	**12960 ±240**	104.1 ±3.5
T1-4	2.800	179.7 ±0.4	1264 ±21	292 ±6	105.2 ±3.2	0.1244 ±0.0018	13020 ±200	**12900 ±210**	109.1 ±3.3
T1-247-249	2.913	202.3 ±0.3	1318 ±11	315 ±3	105.7 ±1.8	0.1243 ±0.0009	13000 ±105	**12880 ±130**	109.6 ±1.9
T1-289-291	4.613	182.8 ±0.3	1832 ±11	206 ±2	102.2 ±1.9	0.1250 ±0.0009	13120 ±102	**12940 ±140**	106.0 ±1.9
T1-5	6.113	216.8 ±0.5	2006 ±20	225 ±3	101.5 ±2.8	0.1259 ±0.0015	13230 ±170	**13060 ±190**	105.3 ±2.9
T1-346-350	7.013	217.1 ±0.3	6155 ±17	74.8 ±0.5	102.3 ±1.5	0.1284 ±0.0008	13500 ±100	**12990 ±270**	106.1 ±1.6
T1-401-405	9.213	187.3 ±0.3	3969 ±11	100.4 ±0.7	104.5 ±1.5	0.1289 ±0.0008	13520 ±90	**13140 ±210**	108.4 ±1.6
T1-6a	9.713	214.7 ±0.5	5990 ±36	77 ±1	103.2 ±2.9	0.1293 ±0.0021	13580 ±240	**13080 ±340**	107.0 ±3.8
T1-6b	9.913	213.6 ±0.5	9162 ±53	51 ±1	101.4 ±3.5	0.1322 ±0.0023	13930 ±260	**13160 ±460**	105.3 ±3.7
T1-7a	10.413	219.8 ±0.5	11070 ±53	44 ±1	102.8 ±3.6	0.1340 ±0.0022	14110 ±250	**13210 ±520**	106.7 ±3.8
T1-7b	10.413	226.2 ±0.6	16160 ±62	32 ±1	108.7 ±3.6	0.1389 ±0.0021	14590 ±240	**13300 ±680**	112.9 ±3.8
T1-7c	10.413	238.0 ±0.6	11670 ±50	45 ±1	104.1 ±3.2	0.1340 ±0.0019	14100 ±210	**13220 ±490**	108.0 ±3.3
T1-8a	10.813	206.0 ±0.4	11380 ±50	41 ±1	104.4 ±2.9	0.1376 ±0.0020	14500 ±230	**13500 ±550**	108.4 ±3.0
T1-8b	10.813	244.2 ±0.5	5620 ±32	94 ±1	100.6 ±2.9	0.1309 ±0.0016	13800 ±200	**13390 ±290**	104.5 ±3.0
T1-9a	11.813	260.4 ±0.6	4330 ±24	138 ±2	111.0 ±2.7	0.1385 ±0.0016	14510 ±180	**14220 ±230**	115.6 ±2.8
T1-9b	11.813	245.6 ±0.5	9990 ±42	59 ±1	113.4 ±2.7	0.1460 ±0.0017	15310 ±200	**14580 ±410**	118.2 ±2.8

References:

Alley, R.B., Meese, D.A., Shuman, C.A., Gow, A.J., Taylor, K.C., Grootes, P.M., White, J.W.C., Ram, M., Waddington, E.D., Maylewski, P.A., and Zielinski, G.A., 1993, Abrupt increase in Greenland snow accumulation at the end of the Younger Dryas event: Nature, v. 362, p. 527-529.

Cheng, H., Edwards, R.L., Hoff, J., Gallup, C.D., Richards, D.A., and Asmerom, Y., 2000, The half-lives of uranium-234 and thorium-230: Chemical Geology, v. 169, p. 17-33.

Edwards, R.L., Chen, J.H. and Wasserburg, G.J., 1987, U-238, U-234, Th-230, Th-232 systematics and the precise measurement of time over the past 500,000 years: Earth and Planetary Science Letters, v. 81, p. 175-192.

Ghil, M., Allen, M.R., Dettinger, M.D., Ide, K., Kondrashov, D., Mann, M.E., Robertson, A.W., Saunders, A., Tian, Y., Varadi, F., and Yiou, P., 2002, Advanced spectral methods for climatic time series: Reviews of Geophysics, v. 40, doi: 10.1029/2001RG000092.

Shen, C.-C., Edwards, R.L., Cheng, H., Dorale, J.A., Thomas, R.B., Moran, S.B., Weinstein, S., and Edmonds, H.N., 2002, Uranium and thorium isotopic and concentration measurements by magnetic sector inductively coupled plasma mass spectrometry: Chemical Geology, v. 185, p. 165-178.

Sontakke, N.A., Pant, G.B., and Singh, N., 1993, Construction of all-India summer monsoon rainfall series for the period 1844-1991: Journal of Climate, v. 6, p. 1807-1811.

Torrence, C. and Compo, G.P., 1998, A practical guide to wavelet analysis: Bulletin of the American Meteorological Society, v. 79, p. 61-78.